Green Chemistry

PAPER

View Article Online
View Journal | View Issue



Cite this: *Green Chem.*, 2021, **23**, 2471

# Sustainable solvent selection for the manufacture of methylammonium lead triiodide ($MAPbI_3$) perovskite solar cells†

Alexander James Doolin,[a] Rhys Gareth Charles,[a] Catherine S. P. De Castro,[b] Rodrigo Garcia Rodriguez,[a] Emmanuel Vincent Péan,[a] Rahul Patidar,[a] Tom Dunlop,[a] Cecile Charbonneau,[a] Trystan Watson[a] and Matthew Lloyd Davies *[a,c]

Perovskite solar cells have emerged as a promising and highly efficient solar technology. Despite efficiencies continuing to climb, the prospect of industrial manufacture is in part hampered by concerns regarding the safety and sustainability of the solvents used in lab scale manufacture. In this paper, we aim to present a methodology for green solvent selection informed by EHS considerations from the CHEM-21 solvent guide for successful methylammonium lead triiodide ($MAPbI_3$) precursor dissolution. Through the use of this methodology we present a *N*,*N*-dimethylformamide (DMF)-free alternative solvent system for deposition of $MAPbI_3$ precursors (MAI and $PbI_2$) consisting of dimethyl sulfoxide (DMSO), dimethylpropyleneurea (DMPU), 2-methyltetrahydrofuran (2-MeTHF) and ethanol (EtOH). We have investigated 3 candidate solutions with slightly different compositions of these four solvents, all of which produce dense, uniform and pinhole-free perovskite films *via* spin coating. All three candidate solutions (A–C) match the average device efficiencies of the DMF/DMSO control devices (12.4%) with candidate A, which consists of 40% DMSO, 30% DMPU, 20% 2-MeTHF and 10% EtOH (vol%), producing a champion PCE of 16.1% compared to 16.2% for DMF/DMSO (80/20 vol%). Perovskite films cast from the three candidate solutions show improved crystallinity, higher fluorescence emission, and improved crystal size uniformity than those cast from DMF/DMSO. This work aims to: highlight the key solvent parameters which determine effective $MAPbI_3$ precursor dissolution; provide a set of criteria for appropriate alternative solvent selection; and demonstrate the application of green chemistry principles to solvent selection for perovskite photovoltaic manufacturing.

Received 7th January 2021,
Accepted 9th March 2021

DOI: 10.1039/d1gc00079a

rsc.li/greenchem



## Introduction

Since their inception in 2009, perovskite solar cells (PSCs) have undertaken a meteoric rise to prominence with power conversion efficiencies (PCEs) climbing from 3.8%[1] to 25.2%.[2] This record surpasses other thin film photovoltaic (PV) technologies[3] and is approaching the theoretical limit of 33% for a single junction device, rivalling monocrystalline silicon (Si), the PV market leader with record PCE of 26.7%.[4] One of the advantages of lead halide perovskites is that the exciton binding energy is low (~50 meV), resulting in the formation of free charges at room temperature, negating the need for an interface to facilitate charge separation.[5] Lead halide perovskites for use in solar cells have an $ABX_3$ crystal structure where A is an organic cation (methylammonium $CH_3NH_3^+$), B is a metal cation ($Pb^{2+}$) and X is a halogen anion ($I^-$, $Cl^-$, or $Br^-$). Tuning the double and triple cation compositions can increase the stability and PCE *e.g.* through the addition of caesium ($Cs^-$), rubidium ($Rb^-$) and formamidinium ($FA^+$) ions into the perovskite crystal lattice. This compositional flexibility results in the ability to tune the band gap ($E_g$),[6] which is generally minimised for optimised light harvesting across the visible-NIR spectrum.[7] Simple solution-based processing and the potential printability of perovskites to create uniform films with reduced defects at low-cost and high throughput gives appeal to manufacturers seeking to commercialise PSCs, including within tandem modules. With record efficiency of

[a]*SPECIFIC IKC, Materials Research Centre, College of Engineering, Swansea University, Swansea, UK. E-mail: m.l.davies@swansea.ac.uk*
[b]*KAUST Solar Centre, Physical Sciences and Engineering Division (PSE), Materials Science and Engineering Program (MSE), King Abdullah University of Science and Technology (KAUST), Thuwal, Kingdom of Saudi Arabia*
[c]*School of Chemistry and Physics, University of KwaZulu-Natal, Durban, South Africa*
†Electronic supplementary information (ESI) available. See DOI: 10.1039/d1gc00079a

up to 29.1%,[2] and the potential to exceed 30% in the near future, tandem devices show great promise as a commercial application for perovskites.[8] Previous studies estimate manufacturing costs for standalone perovskite devices to be half that of Si-PV.[9] These economic advantages over alternative PV technologies may be further enhanced through lifecycle optimisation and design for circular economy enabling remanufacturing of cells and recovery of cell components at lower cost than purchasing new ones, which will afford lower cost devices over successive product generations.[10–12]

In the interests of eco-design, the use of hazardous and high environmental impact materials must be minimised throughout PV lifecycles.[10,13] Access to critical raw materials (CRMs) may also limit the deployment of renewable energy technologies and so where possible these should be substituted for more abundant materials or secondary raw materials, which don't raise the same materials security or conflict mineral issues and may be obtained with considerably lower environmental impact.[12,14–19] On this basis, multiple components present in highly efficient PSCs reported to date require substitution *e.g.* gold and indium; as well as the solvents used to deposit thin-films during manufacture and potentially recovering those same materials in future recycling processes *e.g. N*,*N*-dimethylformamide (DMF) for perovskite and chlorobenzene for spiro-OMeTAD.[20–22]

Traditionally, methylammonium lead triiodide ($MAPbI_3$) has been used as the light absorber layer in PSCs, deposited as a solution of the precursor compounds, MAI and $PbI_2$, in DMF.[23] The presence of lead of in perovskite compositions is a hotly debated sustainability issue within the perovskite sphere. Lead, as a toxic chemical with a propensity to bioaccumulate, especially in aquatic ecosystems, may require substitution for an alternate metal cation. However, currently there are no alternatives that have replicated the high power conversion efficiencies of lead based perovskites. Several alternatives have been identified as potential replacements for lead ($Pb^{2+}$), including germanium ($Ge^{2+}$), bismuth ($Bi^{3+}$), and tin ($Sn^{2+}$). Of these competitor cations, $Sn^{2+}$ is the most promising with a recorded certified efficiency of ~13%.[24] However, the oxidation of $Sn^{2+}$ to $Sn^{4+}$ remains a significant issue with $MASnI_3$ perovskite compounded by low defect tolerance, juxtaposed to the unique highly defect tolerant $MAPbI_3$.[25] Life cycle assessment (LCA) studies have also questioned the perceived benefits of a substitution from lead to tin,[26] with lead presenting a lower embedded energy than tin and problems associated with the toxicity of tin to aquatic environments. Aside from substitution, effective module encapsulation has been posited as a means for mitigating any potential release of lead from future devices, with the expectation of lead based encapsulated devices becoming a commercialised technology. We believe that the issues from the use of lead can potentially be managed through circular economy approaches to mitigate potential impacts arising from the use of perovskite modules throughout their entire lifecycle.[19] Given the current lack of alternatives to lead, and the superior performance of lead based perovskites, significant environmental and sustainability gains could be made from developing alternatives to the DMF solvent system, especially given the likely commercialisation of this technology in the near future. In addition to DMF, several alternative dipolar aprotic solvents for perovskite deposition have been used including γ-butyrolactone (GBL),[21,27] dimethyl sulfoxide (DMSO),[23,28] *n*-methyl-2-pyrrolidone (NMP),[29] and dimethylacetamide (DMAc)[30] with final film morphology and device performance varying due to differences in crystallisation dynamics between solvents.[28] Despite the range of solvents from which $MAPbI_3$ can be successfully deposited, highly efficient devices still rely on DMF based precursor solutions. Reproductive toxicity issues and a workplace exposure limit of 15 mg $m^{-3}$ hinders the scalability of DMF for low-cost manufacturing.[31,32] It has also been proposed that the role of DMSO in lab scale cosolvent systems is vital for high efficiency devices due to enhanced system coordination effects.[33] A crucial challenge of solvent system engineering to support PSC development is to advance understanding of dissolution and coordination of $MAPbI_3$ precursors.[34,35] The impact of solvent fluid properties and colloidal metal–ligand configuration on device PCE should be ascertained to inform the selection of appropriate alternative sustainable solvents and improve the potential for large scale manufacturing.

Several guides evaluating the validity of solvent selection have previously been reported.[36–42] Solvent selection based on environmental, health and safety (EHS) considerations in the absence of full lifecycle assessment has been conducted by numerous large chemical and pharmaceutical firms in the last decade including Sanofi, GSK, AstraZeneca and Pfizer.[40,43–46] Subsequently, researchers have created unified guides consolidating this information, in part due to differences in the priorities of the organisations producing them.[42,47–49] A major effort in this field was the creation of the innovative medicines initiative (IMI)-CHEM21 selection guide,[50] which has been used to guide this research. In addition to EHS considerations, solubility parameters help to identify suitable solvents for dissolution of perovskite precursors. The Hansen solubility parameter (HSP) has been applied in previous attempts to screen alternative solvents,[27,28] to identify solvents similar in Hansen space to DMF, DMSO, NMP, and DMAc. HSP attempts to quantify the solvating power of a solvent in relation to a specific solute by analysing the physicochemical properties of the system with respect to; molecular dispersion ($\delta_D$), dipolar interactions ($\delta_P$), and hydrogen bonding ($\delta_H$).[51]

Wang *et al.* (2017) compiled HSP data for commonly used $MAPbI_3$ precursor solvents and calculated the distance in Hansen space between the solvent and the assumed parameters of the lead iodide solute.[28] However, current theory indicates that HSP fails to account for ionic interaction between perovskite precursors and complexation in solution which prevents accurate application of the Hansen model to $MAPbI_3$ precursor dissolution.[28] Higher solvent polarity has, however, been linked to greater $PbI_2$ salt miscibility,[27] potentially aiding an increase in the concentration of precursor solutions. However, several notable highly polar solvents such as ethylene carbonate do not dissolve $PbI_2$ in contradiction to

 

this theory, indicating influence from multiple solvent properties.[34] Hamill *et al.* (2017) indicated a distinct correlation between the Gutmann donor number ($D_N$), a basicity measure of the solvent, and the ability of the solvent to coordinate $Pb^{2+}$ from $PbI_2$ in solution.[34] Dissolving and retaining adequate concentrations of $PbI_2$ in solution for coating requires solvents which act as strong metal ligands.[52] DMSO was first proposed as a ligand additive with the poorly coordinating solvent GBL to retard crystallisation through the formation of an intermediate phase.[53] Lee *et al.* (2016) expanded on this theory suggesting that $MAPbI_3$ dissolution and deposition is dependent on Lewis acid–base interactions, where $PbI_2$ acts as a Lewis acid with a dipolar aprotic solvent Lewis base donor ligand.[23]

Previous investigations of alternative solvent systems for spin coating, employed to improve sustainability, uniformity, and decrease defect densities have been reported. These include utilising methylamine gas as a post-treatment;[35] DMSO, 2-methylpyrazine (2-MP), and 1-pentanol (1-P) based inks;[28] and GBL, alcohol, cyclic carbonate and acid systems[27] (Table 1). Novel engineering solutions to this problem have been demonstrated, such as dissolving methylamine gas into an appropriate carrier solvent such as acetonitrile (ACN) to successfully deposit functional perovskite films.[52] This utilises strongly basic methylamine which in turn acts as the solvating agent for $PbI_2$. A further application of this method bubbles methylamine through ethanol, which is subsequently mixed with tetrahydrofuran (THF),[54] a common low-cost solvent with high vapour pressure at room temperature, allowing rapid crystallisation over relatively large areas. Both of these systems use volatile bulk solvents and have found application in lab based roll to roll (R2R) manufacture. Due to limited options for DMF alternatives and understanding of the impacts of solubility parameters and crystallisation kinetics in these solvents, further investigation of $MAPbI_3$ deposition with available 'green' and safer solvents along with life cycle impact consideration is required to identify suitable and sustainable alternatives.

A crucial factor to consider is the deposition method used to coat precursor solutions onto substrates. Currently, the highest PCE devices are spin-coated at lab scale, with typical active areas of <1 $cm^2$,[3] whereas alternative methods with superior deposition efficiency are used for scaled-up production such as slot-die coating, spray deposition or inkjet printing for R2R production. Each technique requires specific consideration of the solvent parameters along with the physical and rheological properties that may differ from those of solvent systems developed for spin-coating.[57,58]

Evidence suggests the reaction mechanism between $Pb^{2+}$ ions and a dipolar aprotic solvent results in effective dissolution of trihalide perovskite layers.[36] Due to the required dissolution of lead iodide, alternative dipolar aprotic solvents were shortlisted preferentially as Lewis basic ligands for solvation. When selecting solvent substitutes, primarily driven by EHS concerns, a balance needs to be achieved between performance and 'green' credentials. This requires a methodology to accurately rank respective solvents both in terms of EHS concerns and lifecycle impact considerations, whilst also performing characterisation of the perovskite layer as utilised within a competitively efficient device. DMSO is commonly used as a co-solvent and shows promise in sustainable precursor formulations due to its lack of carcinogenic, mutagenic and reprotoxic (CMR) properties. However, a high boiling point and low vapour pressure limit its use in doctor blading and R2R slot die manufacturing, where more volatile non-coordinating solvents are favoured for near room temperature annealing.[59] A candidate list of commercially available alternative 'green' solvents, regardless of their polarity or hydrogen bonding affinity, was compiled. Consideration of boiling point and flash point was undertaken with these solvents pending industrial evaluation and mitigation by added cosolvents. The aim of this study was to identify commercially available 'green' solvents with desirable properties for the spin coating deposition of $MAPbI_3$ precursor solutions and evaluate their performance. We present a solvent screening methodology based on Hansen solubility metrics, donicity, and EHS considerations. Utilising this method, an alternative solvent system consisting of DMSO, 1,3-dimethyltetrahydro-2(1*H*)-pyrimidinone, also known as dimethylpropyleneurea (DMPU), 2-methyltetrahydrofuran (2-MeTHF) and ethanol (EtOH) is presented and analysed. Furthermore, solvent engineering techniques have been applied to spin coat highly efficient films *via*

**Table 1** Previously published power conversion efficiencies for $MAPbI_3$ solar cells produced from non-DMF $MAPbI_3$ precursor solutions

| Solvent System | Configuration | PCE% | Active area ($cm^2$) | Ref. |
|---|---|---|---|---|
| Acetonitrile/methylamine | FTO/c-$TiO_2$/C60/PAL/Spiro-OMeTAD/Ag | 18.0% Stabilised | 0.09 | 52 |
| | | 15% | 0.7 | |
| Dimethylsulfoxide/2-methylpyrazine/1-pentanol | ITO/c-$TiO_2$/PAL/Spiro-OMeTAD/Au | 16.0% stabilised | 0.09 | 28 |
| μ-Butyrolactone + alcohols/carbonate/acid | ITO/c-$TiO_2$/PAL/Spiro-OMeTAD/Au | 15.1% | N/A | 27 |
| | | 11.9% | 4 | |
| Tetrahydrofuran + ethanol/methylamine | FTO/c-$TiO_2$/m-$TiO_2$/PAL/Spiro-OMeTAD/$MoO_x$/Ag | 20.0% | 0.1 | 54 |
| | | 15.6% | 10 | |
| 2-Methoxyethanol | ITO/PEDOT:PSS/TANP/PCBM/LiF/Al | 15.3% | 0.09 | 55 |
| *N*-Methyl-2-pyrrolidone | ITO/$NiO_x$/PAL/$PC_{61}BM$/Zr(acac)$_4$/Ag | 16.0% | N/A | 29 |
| *N*-Methyl-2-pyrrolidone/dimethylacetamide | Unknown | 17.38% | N/A | 56 |
| Dimethylpropyleneurea as up to 10 vol% additive in dimethylformamide/dimethylsulfoxide | Unknown | ~2% increase | N/A | 34 |

a prenucleation method, optimising the candidate systems of different % compositions showcasing the potential versatility of a 'green' solvent toolbox.[23,34] Structural and optical studies were undertaken to elucidate the crystalline and photoluminescent nature of this novel perovskite. The manufacture and characterisation of full devices based on the optimised DMF-free solvent system aims to shed light on the link between solvent properties and PSC performance.

## Experimental

### Selection of candidate solvents

The process used for screening candidate solvents is outlined in Fig. 1. Initial screening to identify dipolar aprotic solvents with similar properties to DMF was conducted. Polarity, as described by the dielectric constant was considered in initial screening to filter candidates as a majority of known solvents for use in perovskites have dielectric constants above 30, however, high polarity alone is not sufficient.[34] A further indicator used in screening was HSP. Although calculation of the Hansen distance was done using assumed parameters for lead iodide. More recently, the Hansen sphere of lead iodide was described using Hansen Solubility Parameters in Practice (HSPiP) commercial software by Babaei *et al.* (2018).[60] A table showing the results of Hansen distance (HD) calculations using these updated parameters can be seen in Table S2,† with the Hansen distance[28] a function of the parameters relative to the lead iodide salt given by eqn (1).[61]

$$\mathrm{HD} = \sqrt{4(\delta_{D1} - \delta_{D2})^2 + (\delta_{P1} - \delta_{P2})^2 + (\delta_{H1} - \delta_{H2})^2}. \quad (1)$$

### Screening based on environmental, health and safety considerations (EHS)

EHS concerns were used to grade candidate solvents using the IMI-CHEM21 guide (Table 2). Solvents that scored either 'hazardous' or 'highly hazardous' were excluded. Solvents which scored 'problematic' or 'recommended' status as the

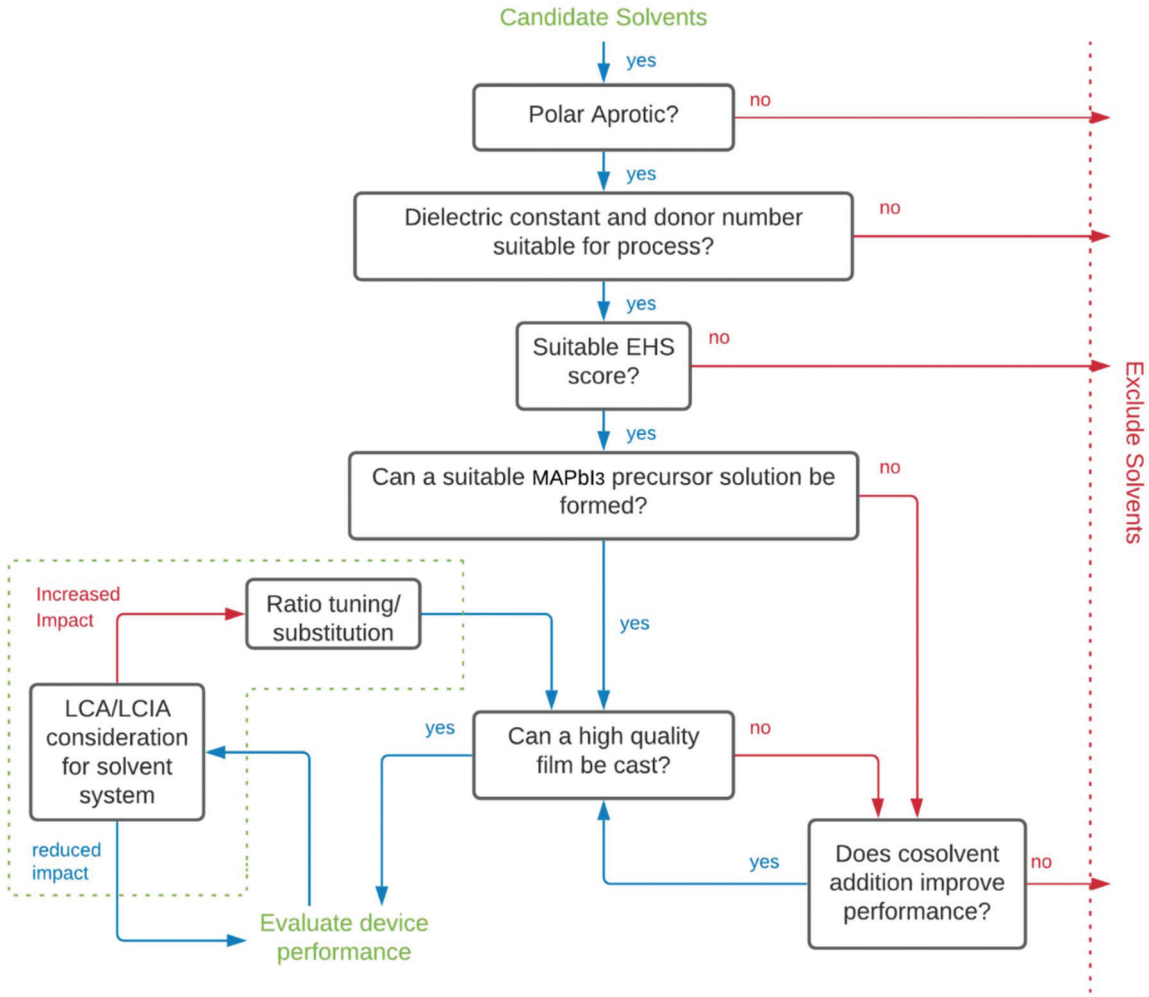


Fig. 1 Solvent selection decision tree for screening and evaluation of alternative solvents. LCA/LCIA evaluation highlighted as a section that requires significant improvement and implementation when considering solvent systems. EHS – Environmental, health and safety, LCA – life cycle assessment, LCIA – life cycle impact assessment, $MAPbI_3$ – methylammonium lead triiodide.

 

Table 2 Traffic light scores of classic PSC solvents vs. alternatives and components (comp) of proposed novel solvent system evaluated *via* CHEM21 method.[50] S – Safety: H – health: E – environment

| Solvents | S | H | E | Outcome |
|---|---|---|---|---|
| **Classic PSC solvents** | | | | |
| DMF | 3 | 9 | 5 | Hazardous |
| Chlorobenzene | 3 | 2 | 7 | Problematic |
| DMSO | 1 | 1 | 5 | Recommended |
| Ethyl acetate | 5 | 3 | 3 | Recommended |
| **Potential alternative aprotic solvents** | | | | |
| 2-MeTHF | 6 | 5 | 3 | Problematic |
| Acetonitrile | 4 | 3 | 3 | Problematic |
| Cyrene | 1 | 2 | 7 | Problematic |
| Dimethyl carbonate | 4 | 1 | 3 | Recommended |
| Ethylene carbonate | 1 | 2 | 7 | Problematic |
| NMP | 1 | 9 | 7 | Hazardous |
| Propylene carbonate | 1 | 2 | 7 | Problematic |
| DMPU | 1 | 6 | 7 | Problematic |
| **Our System** | | | | |
| DMSO (Comp 1) | 1 | 1 | 5 | Recommended |
| DMPU (Comp 2) | 1 | 6 | 7 | Problematic |
| 2-MeTHF (Comp 3) | 6 | 5 | 3 | Problematic |
| EtOH (Comp 4) | 4 | 3 | 3 | Recommended |

outcome of the evaluation were included as a potential improvement on DMF which is determined to have 'hazardous' status.

The task of evaluating solvents on their 'greenness' is complicated by a lack of available lifecycle impact assessment (LCIA) data for emerging green solvents, an issue that is commonly encountered attempting to conduct lifecycle assessment (LCA) on green solvents.[62] For DMPU this data remains unavailable due to limited industrial application. Full consideration of the trade-offs in environmental impacts at different stages of product lifecycles resulting from solvent substitution is not possible without it, or a better picture of all processes involved in manufacturing, distribution, use, collection and end-of-life stages of PSC products. However, consideration of available LCA data showing cradle to gate impacts of solvents has been considered.

### Technical evaluation of candidate solvents

Following EHS screening, remaining candidate solvents were purchased from Sigma-Aldrich (anhydrous solvents where possible, used as received) and 1st generation precursor solutions were made by adding $PbI_2$ (~580 mg) and MAI (~200 mg) in 1 mL of candidate solvent by heating to 60 °C with stirring. If the precursors remained undissolved, temperatures were increased until complete dissolution was achieved, or the solvent could be excluded for failing to dissolve precursors to a sufficient extent to achieve a 1.25 M solution. In such cases, undesirable reactions often resulted from solvent–solute or solute–solute interactions.

### Manufacture of devices

All devices were manufactures in a glovebox environment. Candidate precursors solutions were used to fabricate PSCs with n–i–p planar configuration (FTO/$SnO_2$/$MAPbI_3$/Spiro/Au), using tin oxide as an electron transport layer, chosen for superior stability whilst also maintaining high electronmobility.[63] The control system consisted of DMF (Acros Organics extra dry $HCON(CH_3)_2$ 99%) and DMSO (Acros Organics extra dry $(CH_3)_2SO$ 99%) in a 4 : 1 ratio. A 1 mL $MAPbI_3$ solution consists of 576 mg of lead iodide ($PbI_2$, TCI Chemicals 99.99%), 199 mg methylammonium iodide ($CH_3NH_2$·HI 98%).

Heating at 60 °C and rigorous mixing was applied to the DMF/DMSO $MAPbI_3$ solution to aid precursor dissolution. The candidate solutions used the bulk cosolvent system of DMSO and DMPU (Sigma Aldrich, absolute, over molecular sieve, $H_2O \leq 0.03\%$, ≥99% GC) with solvent additives 2-MeTHF (Sigma Aldrich, bio-renewable, anhydrous, ≥99%, inhibitor free) and EtOH (Sigma Aldrich, absolute, 99%, extra pure, SLR). Heating at 80 °C was applied to the candidate solutions (A, B, and C), along with rigorous mixing until the complete dissolution of the precursor materials.

A tin oxide solution was prepared from a commercially available 15% tin(IV) oxide colloidal solution (Alfa Aesar) which was diluted by a ratio of 2.6 : 1 with deionised water and sonicated for half an hour. 85 mg of the hole transport material 2,2′,7,7′-tetrakis–(*N*,*N*-di-4-methoxyphenylamino)-9,9′-spirobifluorene (Spiro-OMeTAD – Merck Millipore – Sigma Aldrich) was dissolved in 1 mL chlorobenzene (anhydrous, 99.8%) with 34 μL 4-*tert*butylpyrridine and 20 μL of bis(trifluoromethane) sulfonimide lithium salt (Li-TFSI) in acetonitrile (520 mg Li-TFSI in 1 mL acetonitrile (anhydrous, 99.8%)). The completed hole transport layer (HTL) solution was then filtered with 0.2 μm PTFE (polytetrafluoroethylene) membrane filter before deposition.

Pre-cut laser etched 2.8 $cm^2$ pieces of XOP fluorine doped tin oxide (FTO) Glass (tec15–2.2 mm thick) were first cleaned with 2% hellmanex solution, before being sonicated for 30 minutes at 70 °C in a 2% hellmanex solution, followed by sonication for 5 minutes in deionised water at 70 °C. Substrates were transported to a class 6 clean room environment for 30 minutes sonication in acetone and IPA respectively prior to drying with a nitrogen flow and followed by 10 minutes treatment in a plasma cleaner at maximum power using oxygen at 0.3 mbar. A 10 minutes UV-Ozone treatment was conducted prior to $SnO_2$ deposition with time between the UV-Ozone treatment and $SnO_2$ deposition minimised. Prior to coating, the spin-coater (in the class 6 environment), was wiped with deionised water to ensure higher humidity.[64] 150 μL of tin oxide solution was spin coated onto substrates dynamically at 3000 rpm and 3000 acceleration for 30 seconds with solution dropped onto the sample after 5 seconds. Immediately after, a swab was used to remove a strip of the $SnO_2$ before annealing at 150 °C for 30 minutes on a hot plate to remove all moisture. A one hour UV-Ozone treatment was applied to the electron transport layer (ETL) substrate to reduce hysteresis.[65] Samples were then transferred to a glovebox for perovskite deposition. The one step deposition method was used to spin coat $MAPbI_3$ solutions onto substrates with an anti-solvent drip of ethyl acetate (EA) to initiate nucleation

and crystallisation growth of the film. For the reported control solution (DMF/DMSO 80/20 v/v), spin coating setting of 4000 rpm, 4000 acceleration for 30 seconds were used. 200 μL of ethyl acetate was dropped onto the sample 7 seconds from the start of the spin cycle. Samples were then placed on a hot plate at 60 °C and ramped rapidly to 100 °C for 10 minutes to anneal. For the candidate solutions, a prenucleation method of spin coating was used, harnessing the antisolvent drip stage during spin coating to induce the nucleation and crystallisation of the wet film. This method was used to form dense, pin hole free, specular films given the difference in solvent system properties to the control solution. It was thought that the standard control spin coating methodology leads to high defect levels if a transparent intermediate phase is formed from the candidate solutions due to over-coordination and poor solvent evacuation from the film. A specular layer was formed using a two-stage spin setting of 10 seconds at 1000 rpm with 200 acceleration, followed by 30 seconds at 6000 rpm 2000 acceleration. In this case 200 μL of ethyl acetate was dropped five seconds from the end of the cycle by application of slow continuous pressure to the pipette for ~2 seconds resulting in a semi-transparent brown sample post spin-coating, which was immediately annealed on a hot plate at 100 °C for 10 minutes. 100 μL of Spiro-OMeTAD solution was dropped on to the device stack dynamically, 10 seconds before the end of the 4000 rpm, 30 seconds spin cycle. Oxidation of the HTL was achieved through leaving the device in a dark environment for 12 hours. Finally, gold wire (Au, 99.99% purity 1.0 mm thick Sigma Aldrich) used to deposit top contacts on devices using an Edwards bell jar evaporator at a pressure of $10^{-5}$ mbar.

### Cell performance evaluations

The current–voltage (*J*–*V*) curves of devices were recorded using an Oriel Sol3A solar simulator, under simulated AM1.5 sun illumination. A shadow mask defined an active area of 0.09 $cm^2$ for each evaluated pixel. A total of 8 pixels were evaluated per sample with a pre-sweep delay for light exposure of 1s, and a sweep time of 9.8s through the range 1.2 V to −0.1 V. The data presented was obtained from the reverse scan set up.

Published procedures for the use of $SnO_2$ as an ETL on FTO recommend chemical bath deposition.[66] In this study the ETL was spun on FTO from a nanoparticle solution. It was postulated that due to the inherent surface roughness of the FTO (FTO having a root mean square value of 16 nm in comparison 0.63 nm for indium doped tin oxide (ITO)[67]), the ETL exhibited poor surface coverage. This led to erratic open circuit voltage between pixels on the same sample. A recommendation is to use ITO in this build procedure when surface roughness cannot be altered by modification methods. As the lower cost indium-free alternative to ITO, FTO may still be used in this architecture provided that a consistent, pin hole free, tin oxide transport layer be deposited. In order to attain comparable results between devices/solvent systems all data was analysed and evaluated pixels with a recorded open circuit voltage below 0.85 V were omitted.

### Optical evaluations

As these films were made in ambient conditions, the EA antisolvent drip timing was changed to 15s from the start of the cycle (from 7s) for the control with the 'prenucleation' strategy remaining as described. Absorptance and fluorescence measurements of thin films were made using an Edinburgh instruments FS5 spectrofluorometer, with the standard thin film sample holder; the integrating sphere unit was used to measure absorptance. Fluorescence (excitation wavelength of 450 nm) was measured using an integrating time of 0.2s and 3 nm excitation and emission slits. Measurements were taken on films in the absence of the transport layers and contact (*i.e.* FTO/$MAPbI_3$/PMMA). This stack was manufactured in ambient conditions with the poly(methyl methacrylate) (PMMA – Sigma Aldrich, average molecular weight ~120 000 by GPC) layer spin coated onto the perovskite film to prevent environmental degradation during the measurement. PMMA (1 : 1 by weight with toluene) was deposited *via* spin coating at 3000 rpm (3000 acceleration) for 30 seconds, followed by a 3 minutes anneal at 70 °C. For consistency, samples were placed in the dark sample holder prior to measurement for 2 minutes. Three films per solution were evaluated with repeat measurements under constant illumination to mitigate the effect of photobrightening.[68] To achieve this, measurements were taken with a 2.5 minutes delay of light exposure between scans until the scans converged and were deemed 'stable' (see Fig. S6† for candidate A solution multiple scan results). The uncorrected 'stable' scan for each sample was used when calculating the average data shown in Fig. 5 along with the standard deviation range from the mean shown by the shaded region. Absorptance scans were taken using the same sample architecture in the integrating sphere. Slit widths of 2.5 nm on the excitation and 0.25 nm on the emission were used for both the blank sphere scan and with the sample in the direct position. A synchronous scan was completed first on the blank sphere over the wavelength range 450–850 nm providing a baseline measurement. Subsequent to this, with the sample in the direct position within the sphere, a further synchronous scan was completed over the same range. It is worth noting that the slit widths should be set such that at the wavelength of the Xenon bulb (468 nm) the resulting emission doesn't saturate the detector. The fluoracle software can then be used combining the blank and direct position scan and providing analysis to attain reflectance and absorptance curves. The presented absorptance curves were attained through linear interpolation between the original data points, then smoothed using the Savitzky–Golay method with 6 points in window and a polynomial order of 3 (on OriginPro, 2020b).

### X-Ray diffraction (XRD) analysis

XRD measurements were performed using a Bruker D8 Discover in a standard divergent slit set-up. The sample architecture used FTO/$SnO_2$/$MAPbI_3$/PMMA, with the $SnO_2$ deposited in class 6 clean room conditions followed by $MAPbI_3$ deposition in a nitrogen glovebox environment. The build pro-

 

cedure mimicked the device manufacture simply omitting the HTL for PMMA. The scan range was set from 5–60° and the measurements taken using a 40 kV, 40 mA Copper source with a step size of 0.04°, at 1 second per step. Origin peak analyser was used to find the full width at half maximum for the 110, 220, and 310 characteristic tetragonal $MAPbI_3$ peaks. This was done by subtracting the baseline and integrating 0.5 degrees either side of the peak.

### Scanning electron microscopy (SEM) imaging

SEM images were taken using a JEOL 7800F FEG-SEM with 30 000× magnification. 5000×, 10 000×, 15 000× images are available in Fig. S1–S4.† Machine learning based image analysis was undertaken using the Zen Blue Intellesis module software. 30 000× magnified images were used to manually train the module to segment the image as the perovskite crystal (object) and the respective grain boundaries (the background). The images were enhanced to increase contrast enabling the software to segment the image for further analysis (Fig. 2). Once the image analysis software segmented the crystals, incomplete crystals or those with no clearly defined boundary were manually extracted during the analysis phase defining measurement regions. Parameters including area, perimeter, diameter, roundness, and maximum Feret diameter were taken for each complete segmented crystal available using the Zen Blue image analysis module with the results presented in Table S5.† Errors given for crystal size parameters represent 1 standard deviation in size from the mean in nm.

### Profilometry

Film thickness was measured using a KLA Alpha-Step D-600 stylus profiler. Films were manufactured in a nitrogen glovebox on FTO after 10 minutes of UV-Ozone treatment and cleaning as per the manufacture method. A thin strip was manually scraped from the middle of the film to allow step down measurement of the surface. Each measurement was taken step down over a 3 mm distance with the average results presented in the Table S3.† Fig. S9† provides a graphical representation of the base data attained for the measurement of a ~500 nm thick film deposited using the candidate A solvent system.

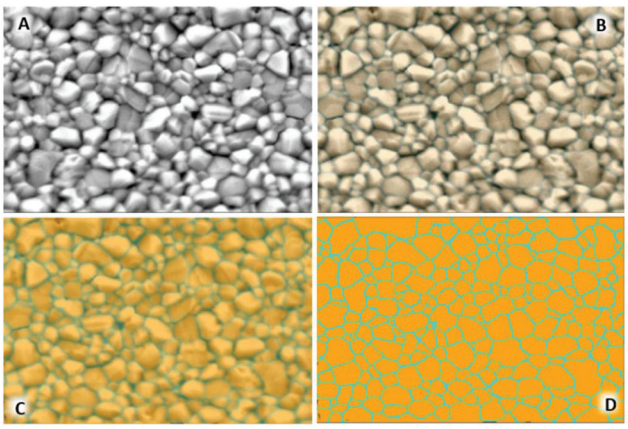


Fig. 2 SEM of $MAPbI_3$ thin-film deposition from candidate A solvent system with 30 000× magnification (A) and the Zen Blue image analysis segmentation (B–D). (A) Mirrored image of the base data for the image analysis software to segment. To illustrate the accuracy of the segmentation the label opacity is increased (B–D) with the final result (D) typical of the segmented data analysed to extrapolate crystal size characteristics.

## Results and discussion

The process of solvent selection is complicated by competing concerns relating to sustainability, health and safety, and cost; ultimately this relates to the viability of cost effective manufacture. Current theory suggests that competitively efficient perovskite films (*ca.* 25%) rely on strongly coordinating organic solvents. Conversely these solvents tend to grade low in terms of both sustainability and health and safety factors. Industrial manufacturing concerns may also alter the emphasis where solvent cost may be mitigated by effective solvent capture and reuse. However, where solvent capture is applied, large capital expenditure (CapEx) costs can be anticipated for more toxic chemicals. It is also worth noting that the cost of alternative solvents is much higher than traditional solvents (Table 3 and Table S1†). Currently, this cost disparity becomes even greater at high volumes as traditional organic solvents have more developed production routes benefitting from economies of scale, whereas emerging solvents may have more complex synthesis, and are manufactured at smaller scale with higher associated costs. Considering the relative CapEx requirement, a low toxicity solvent system could end up a more cost effective option in the intermediate and longer term as the alternate solvent production routes develop and also benefit from economy of scale. Table 3 reports the 'greener' aprotic polar solvents *i.e.*, those that scored 'problematic' or 'recommended' following EHS evaluation with the CHEM21 method, along with further a justification for their consideration for application in PSC production. Recent advances in the area of perovskite solvent impact include the analysis provided by Vidal *et al.*, 2020. This research considers the health and environmental impact of several commonly used perovskite solvents in terms of both solvent production and energy demands alongside application of the 'USEtox' method to assess the wider health impact of each solvent.[69] This work highlights the importance of the comparatively benign organic solvent DMSO and underlines the toxicity concerns surrounding most other commonly used solvents including DMPU. These concerns are relative to the placement of DMF on the candidate list of substances of very high concern (SVHC) as part of the registration, evaluation, authorisation, and restriction of chemicals (REACH) initiative headed by the European Chemical Agency;[69] however, there is a clear need for comprehensive frameworks to aid in the design of genuinely green and low toxicity solvent systems that attain high PCE. Based on Hansen parameter evaluation (Table S2†), several solvents were considered as promising candidates, creating a close position

Table 3 Candidate solvent selection table used to shortlist potential green solvents based on a literature review of green solvents along with varied solvent characteristics

| Solvent | Cost[a] (GBP per L) | Health and safety codes | b.p (°C) | f.p (°C) | Justification for solvent use |
|---|---|---|---|---|---|
| Cyrene | £171.00 | H319 P305 + P351 + P338 P337 + P313 | 203 | 108 | Developed as a green solvent by the Circa Group in conjunction with the Green Chemistry Group.[36] Boiling point is higher than DMF but not drastically and the route of production is far more environmentally friendly as a bio based solvent. Cost is a potential concern as production is currently small scale. |
| Dimethylpropyleneurea (DMPU) | £333.00 | H302, H317, H318, H361 P280, P305 + P351 + P338 | 247 | 120 | Classified as a 'greener' alternative solvent by Byrne 2016.[42] Lacking popularity in industrial applications with concerns regarding cost and the health and environmental impact of the solvent. |
| 2-Methyltetrahydrofuran (2-MeTHF) | £146.00 | H225, H302, H315, H318 | 78 | −11 | Created as a green replacement solvent for tetrahydrofuran (THF). Derived from biomass processes, this solvent exhibits a greener production than THF with far lower toxic effects.[48] |
| Sulpholane | £198.00 | N/A | 282 | 166 | Touted as a green solvent with a high boiling point and corresponding flash point. Some issues noted due to high toxicity, with sources citing mitigation through low skin penetration effects.[38] |
| Cyclopentyl methyl ether (CPME) | £132.00 | H225, H302, H315, H319, H412 | 106 | −1 | Classified by GSK metrics as a substance with 'some issues', despite substitution been requested by Sanofi.[42,43] Issues with sensitivity to light have precluded this solvent from testing in a fume cupboard environment. |
| 1,2,3-Trimethoxypropane (1,2,3-TMP) | No data available | No data available | 143 | 42 | Created as a trimethyl ether of glycerol, the green qualities of the feedstock are attractive. Synthesised for $CO_2$ capture, little is known about the physical properties to date.[70] Due to low boiling point and green feedstock, appears to be a promising candidate on paper. Unavailable for testing due to lack of commercial manufacture. |
| γ-Valerolactone | £374.00 | H227 | 207 | 81 | A bio derived solvent from cellulose feedstock, this represents a promising green solvent in certain industries. Production route is linked to the emergence of the green hydrogen economy.[48] |
| 1,3-Dimethyl-2-imidazolidinone (DMI) | £258.00 | N/A | 225 | 120 | A homolog of DMPU, this solvent has similar characteristics to hexamethylphosphoramide (HMPA), a carcinogenic solvent, and has been used as a green alternative in certain synthesis pathways. This is mainly due to reduced toxicological effects[42] |
| Ethylene carbonate | £112.00 | H302, H319, H373 | 248 | 143 | Previously used as an additive in GBL based solutions. The solvent itself cannot fully solvate the precursors or form the appropriate complexes. The high boiling point excluded this from further investigation. |
| Propanenitrile | £131.40 | H225–H300 + H310–H319–H332 | 98 | 6 | Included in the candidate list to contrast the acetonitrile-based mixtures. The low boiling point suggests a potential co-solvent to aid in solvent removal. Huge toxicity issues surround the use of this from a health and safety perspective. |

[a] The cost of these solvents was taken from Sigma Aldrich at equivalent grade/purity where available. b.p – Boiling point, f.p – flash point.

in Hansen space relative to the estimated HSP sphere of $PbI_2$. Whilst none of the evaluated solvents provided a perfect match, the Hansen distance (HD) of DMSO is 6.7, the smallest evaluated distance. DMF and GBL both show the next closest HD values.

Qualitative experimental data suggests that all three of these solvents are able to dissolve the lead iodide precursor in the presence of MAI, despite the low coordination number of GBL. This provides justification for continued use of DMSO as part of a cosolvating system. EHS solvent screening showed the newly developed solvent cyrene to be a possible dipolar aprotic replacement for DMF. However, our HD evaluation, along with that performed by Wang, *et al.* (2017), suggests that cyrene is relatively far away from lead iodide in Hansen space which may explain the poor performance of cyrene in generation 1 testing, with precursors precipitating out of solution. This is probably due to insufficient polarity and a comparatively low $\delta_H$ value – representative of hydrogen bonding affinity. A low $\delta_H$ value is hypothesized to result from the hydrogen accepting ability of the C=O bond present within the cyrene molecule. The properties of the candidate solvent DMPU are not encouraging based upon this metric. Although the effective use of DMPU in cosolvent systems relies specifically upon its ability to coordinate the metal ion and form a complex, a major aspect of dissolution not accounted for in Hansen evaluation. However, Hansen solubility provides a useful benchmark showing the importance of polarity in relation to the lead iodide salt while pursuing a 'like dissolves like' approach to dissolution.

HSP gives a point of reference for selecting solvents with similar parameters as substitutes.[27,28] Despite the limits to the HSP model, a centralised theory of polarity and coordination

 

impacting effective $MAPbI_3$ precursor dissolution was used to define ideal parameters. The candidate solvents were therefore used in a second level of experimentation incorporating Gutmann donor number theory as a crucial parameter (Fig. 3).

The donor number serves as a quantitative measure of Lewis basicity[71] and has been linked to coordination of the perovskite precursor[34] metal centre $Pb^{2+}$. The challenges inherent to $PbI_2$ dissolution and coordination within a solvent system have been previously studied and were found to be independent of the counterion present[41] (methylammonium in this case). A reduction in the coordinating capacity of the solvent causes an increase in iodine ion concentration which in turn leads to iodoplumbate ion formation[72] of $PbI_3^-$ and $PbI_4^{2-}$. This behaviour enlightens the dissolution process and informs solvent selection further, as inhibition of these mechanisms by increasing the coordinating ability of the solvent may lead to customisation of resulting morphological effects.[34]

DMPU was chosen as a major constituent, effectively replacing DMF, due to the high donor number, along with an adequate dielectric constant – similar in magnitude to DMF. DMPU has previously been studied as a solvent additive with the observation that when used alone to dissolve the precursor materials the coordination of $Pb^{2+}$ leads to a precipitate forming at room temperature.[34] We report this finding through our own studies but found the effect mitigated by adding as little as 10 vol% of DMSO. In order to capitalise on the increased coordinating ability offered by DMPU, the coordination chemistry of the solvated $Pb^{2+}$ complex and the resulting colloidal configuration regarding the space demands of the solvent require further study. Studies suggest DMPU is a particularly space demanding solvent that coordinates lead in a holo-directed octahedral manner, whereas DMF preferentially coordinated in a hemi-directed configuration.[73] Fig. 4 shows a graphical representation combining the desired properties of high donicity and dielectric constant with the region of interest (ROI) highlighted for a DMSO/DMPU cosolvent system.

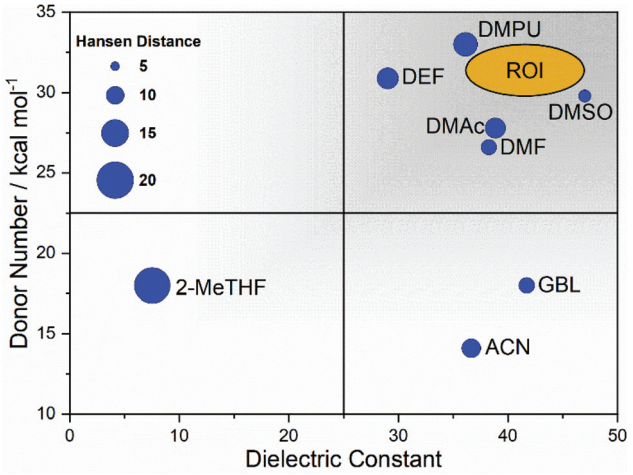


**Fig. 4** Graphical representation showing both the dielectric constant and donicity of several solvents analysed in this study. The selected combination of DMSO and DMPU aims to combine the highest polarity and most strongly coordinating solvents available to dissolve high concentrations of $PbI_2$ needed for spin coating highly efficient $MAPbI_3$ films. The region of interest (ROI) defines the combined donicity and dielectric constant range for the chosen cosolvent system (DMSO/DMPU).

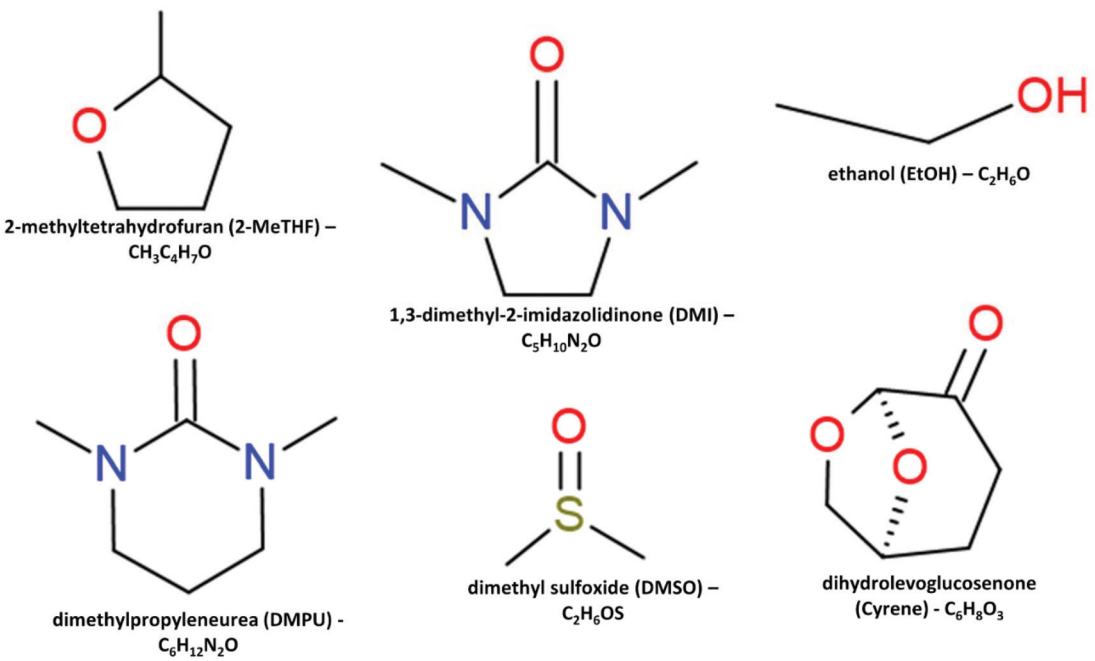


**Fig. 3** Chemical structures of solvents evaluated for perovskite deposition in this study.

In developing an alternative solvent system, we have utilised solvent characteristics ranging from the dielectric constant and HSP, the fluid properties of vapour pressure and boiling point, to the Gutmann donor number ($D_N$) and consideration of solvent space constraints and colloid configuration.

Our initial solvent screening yielded several solvent candidates, including the promising highly coordinating solvents DMSO and DMPU. These solvent candidates were used alone and in combination in several stages of testing to ascertain their ability to dissolve $MAPbI_3$ precursors. Table 4 provides qualitative data evaluating four generations of cosolvent systems. DMPU, showed promise during 1st generation testing, with 1 mL solutions completely dissolved at 1.25 M concentration. Dimethylimidazolidinone (DMI), a homolog of DMPU, was also evaluated with lower observable dissolution of the precursor materials along with a precipitate forming after time exposure. Cyrene (Table 3) was also considered for cosolvent testing due to its promise as a bioderived alternative to traditional dipolar protic solvents. The results for cyrene, 2-MeTHF, and propanenitrile were similar in that black crystalline precipitate formed indicative of $MAPbI_3$ perovskite. These solvents were then excluded from individual use due to an inability to coordinate the $PbI_2$ and prevent the 'crashing out' of perovskite crystals in solution. Based on the initial ability to dissolve the precursors in 1st generation testing, 2nd generation testing involved inhibiting the formation of a solid phase resulting from strong over-coordination of DMPU,[34] by addition of a cosolvent. Attempts were made to improve the prospect of using the green solvent cyrene through the addition of the highly polar and strongly coordinating solvent DMSO. However, this yielded no successful solutions. The 2nd testing phase culminated in the manufacture of films and full devices where possible to ascertain which solvents combinations to pursue. 3rd generation testing proceeded with the best performing systems of DMSO and DMPU from 2nd generation testing, where a tertiary additive was selected to improve performance. Lower vapour pressure or boiling point additives were selected to balance the high boiling point and low vapour pressure of DMSO and DMPU, in alignment with the characteristics of the DMSO/DMF system. 4th generation testing aimed to improve device PCE through ratio and miscibility tuning. The evaluation of these solvent systems is given in Table 4. From the trials 3 candidate solutions (A, B, and C) were selected for further analysis, each contain 40% DMSO where the % composition of DMPU, Me-THF and ethanol are varied. Multiple candidate solutions were formulated based on a core combination of DMSO and DMPU, an historic alternative dipolar aprotic solvent derived to replace hexamethylphosphoramide (HMPA) with a high coordination ability as defined on the Gutmann scale as 33 kcal $mol^{-1}$ compared to 29.8 kcal $mol^{-1}$ for DMSO and 26.6 kcal $mol^{-1}$ for DMF.[74] Of the lower coordinating 'green' solvents 2-methyltetrahydrofuran (2-MeTHF) and ethanol (EtOH), 2-MeTHF can be biologically derived[75] and was selected for high vapour pressure; with EtOH added to improve the miscibility of 2-MeTHF with DMSO/DMPU whilst simultaneously increasing solution supersaturation. This provides a degree of flexibility in developing an efficient solvent system for a given manufacturing procedure.

The concentration of the precursor solution was fixed at 1.25 M for the purpose of spin coating as this is commonly used. The dissolution and coordination of the precursors in the candidate systems is directly dependent on the DMSO/DMPU cosolvent combination. At this concentration, the lowest the DMSO/DMPU ratio possible with successful dissolution was the given ratio for candidate A and B (70% of the total volume). <70% total volume adversely impacts the ability to form a spin coat-able solution in a reasonable time window. The ratio of 2-MeTHF and EtOH has been varied to explore the impact of their respective rheological properties. Candidate C consisted of additional DMSO/DMPU to ascertain the impact of increased coordinative bulk solvent on the produced films with the benefit of increased solution stability and ease of processing.

Having successfully formed stable $MAPbI_3$ precursor solutions the optical and morphological characteristics of spin coated films were studied. Films manufactured from the 3 candidate solutions, show similar absorptance to the control (deposited from DMF/DMSO) with a very slight shift in the band gap position for films manufactured from candidates A and B (Fig. 5). This is less apparent in the photoluminescence spectra; all films show a similar maximum emission wavelength, with only ±1 nm between the average maximum emission wavelength of samples (from the measurements of 3 films per sample, see Fig. S11†). Care is needed in assigning significant differences between these samples to these slight changes in band-gap and maximum emission wavelength, especially given the highly sensitive nature of the photoluminescence from perovskite samples in ambient conditions,[68] these slight differences are likely due to the differences in crystals size.

The three candidate films show slightly higher absorptance and significantly higher photoluminescent intensity, it is worth noting that the absorptance varies less between samples at the excitation wavelength for photoluminescence (PL) measurements (Fig. S7†) and thus the higher PL is not only due to higher absorptance. Since these are thin-films (with no HTL present) and not full devices, higher PL is likely indicative of a lower defect concentration suggesting the candidate solution have produced higher quality films than the control. It is important to note that PL measurements are an average of 3 measurements or 3 films and so the candidate solutions produce films with higher PL consistently. Thicknesses of the films were measured *via* profilometry (Table S3†) giving average values of 366, 487, 492 and 365 nm for the control and A, B, C films, respectively. Solvent systems A and B produce films which are approximately 25% thicker than the control or solvent system C, suggesting that the volume of 2-MeTHF directly affects the final film thickness. This could be due to the higher volatility of 2-MeTHF, which aids in the expedient removal of the solvent after coating.

 

Table 4 Solvent systems evaluated in the initial screening in this study and results of attempts to create precursor solutions (Y – Yes, N – No, DT – dissolution temperature used, PD – precursor dissolution, STP – standard temperature and pressure, control – 80/20 v/v DMF : DMSO solution)

| | Solvent system@1.25M ($MAI + PbI_2$) (vol%) | PD | DT (°C) | System condition at STP | Major characteristics of the solvent system |
|---|---|---|---|---|---|
| 1st Gen | 100% cyrene | N | — | Black precipitate solution, highly viscous | Black solid undissolved, potentially crashing out $MAPbI_3$ crystals |
| | 100% DMPU | N | — | Crystalline solid forms over time | Initial dissolution. Over time the solution solidifies to a crystalline yellow solid, postulated to result from over coordination of the $PbI_2$34 |
| | 100% DMI | N | — | Crystalline solid forms | Dissolution appears weaker than with DMPU, solid forms over time |
| | 100% 2-MeTHF | N | — | Black precipitate solution – low dissolution | Less solvating power than cyrene with a similar black precipitate solution, some orange coloured solid observed indicating lead iodide still present |
| | 100% propanenitrile | N | — | Black precipitate solution | Similar black precipitate that is present for cyrene and acetonitrile |
| 2nd Gen | 20% cyrene, 80% DMF | Y | 60 | Deep orange $MAPbI_3$ solution | Very visible colour change to orange |
| | 20% DMPU, 80% DMF | Y | 60 | Yellow $MAPbI_3$ solution | Equivalent solution to DMF/DMSO visually |
| | 20% cyrene, 20% DMSO, 60% DMF | Y | 60 | Orange colour present – solution forms | Solution does form but orange colour returns during cooling over time |
| | 20% DMPU, 20%, DMSO, 60% DMF | Y | 60 | Yellow solution – similar colour match to control | Equivalent solution to DMF/DMSO visually |
| | 80% cyrene, 20% DMPU | N | — | Solid forms | Reaction system causes solid to form, cyrene susceptible to strong bases |
| | 20% cyrene, 80% DMPU | N | — | Solid forms | Reaction system causes solid to form, cyrene susceptible to strong bases |
| | 50% ACN, 50% DMPU | N | — | Foam like solid forms – fast rate | Quickly turns into a foam like crystalline lattice when spun with vortex |
| | 70% ACN, 30% DMPU | N | — | Crystalline structure and foam like solid present | Slower reaction rate but solid and crystals still form |
| | 10% DMSO, 90% Cyrene | N | — | Polymer like solid forms over time | Reaction occurs |
| | 20% DMSO, 80% Cyrene | Y | 90 | Solution also dark orange in colour | No reaction observed, strong orange red colour solution, quite viscous |
| | 30% DMSO, 70% Cyrene | Y | 95 | less viscous than above solution – crystals form at STP | No reaction observed, strong orange red colour solution, quite viscous |
| | 10% DMSO, 90% DMPU | Y | 110 | Yellow solution – higher apparent viscosity that control | Visually more viscous that control solution, good colour match |
| | 20% DMSO, 80% DMPU | Y | 110 | Yellow solution – lower apparent viscosity than above | Visually more viscous that control solution, good colour match |
| | 30% DMSO, 70% DMPU | Y | 105 | Yellow solution – lower apparent viscosity than above | Visually more viscous that control solution, good colour match |
| 3rd Gen | 20% DMSO, 60% DMPU, 20% PPN | Y | 95 | Yellow solution, good match to control | Visually lower viscosity, possible miscibility issues |
| | 20% DMSO, 60% DMPU, 20% ACN | Y | 100 | Yellow solution with fine crystalline lattice present at STP | When cooled to room temperature overnight a crystal lattice forms. Needle type crystals (likely $PbI_2$) |
| | 20% DMSO, 60% DMPU, 20% 2-MeTHF | Y | 95 | Yellow solution mimics control | Visibly more viscous than the control, possible miscibility issues |
| 4th Gen | **Candidate A** 40% DMSO, 30% DMPU, 20% 2-MeTHF, 10% EtOH | Y | 80 | Yellow solution, improved viscosity match to control | Remains a yellow solution upon cooling. Slight stoichiometric differences between $PbI_2$ and MAI can cause $PbI_2$ to crash out of solution |
| | **Candidate B** 40% DMSO, 30% DMPU, 15% 2-MeTHF, 15% EtOH | Y | 80 | Yellow solution | Some lead iodide precipitate upon cooling to STP over time |
| | **Candidate C** 40% DMSO, 40% DMPU, 10% 2-MeTHF, 10% EtOH | Y | 80 | Yellow solution, slightly higher viscosity than A and B | Precursors remains 'stable' in solution at ambient temperature |

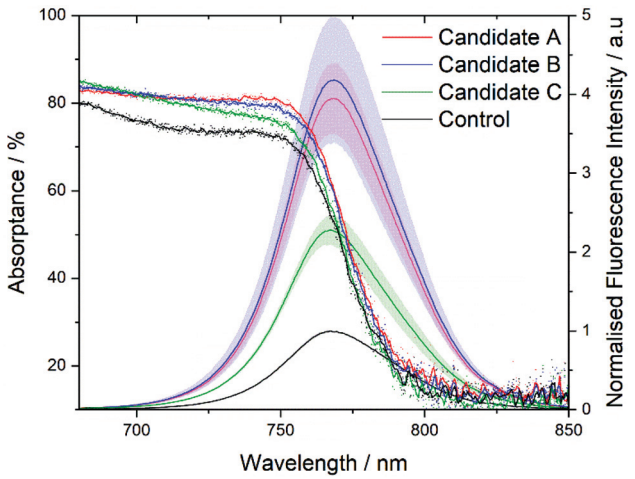


**Fig. 5** Absorptance and photoluminescence – excitation wavelength ($\lambda_{ex}$ 450 nm) for each for films manufactured in ambient conditions from the control and candidate solvents. Three films per solution were evaluated, 3 nm excitation and emission slit widths and repeat measurements under constant illumination were used to mitigate the effect of photobrightening. All curves have been normalised to the maximum value of the control PL curve. The final 'stabilised' curve was used for each sample to create the average curve. The standard deviation of each sample set is displayed as the shaded region (film thicknesses were determined through profilometry with mean average values of: 366, 487, 492, and 365 nm for the control, A, B, and C).

Despite the higher rotations per minute (rpm) during the coating process, candidate films A and B remain considerably thicker than their counterparts. The route of this appears to lie in the method of spin coating itself. In lieu of DMSO adduct intermediate phase formation, a 'prenucleation' method has been used for the candidate solvent systems. This leads to the formation of a phase of perovskite crystal during the spinning operation (light brown colour) with the subsequent annealing step precipitating 3D tetragonal $MAPbI_3$ from the solvent bound film above (as evidenced by XRD analysis). This method appears to lead to thicker films independent of the spin speed used.

SEM of the samples (Fig. 6, left) show both the control and candidate solutions produce a dense, pinhole free, highly compact perovskite film. A difference in spin coating anti-solvent drip methodologies between the control and candidate solutions involves the formation of an intermediate phase as identified as a DMSO based adduct in the DMF/DMSO solution, by which the anti-solvent ethyl acetate (EA) removes the majority of the DMF and leaves a transparent adduct phase which upon annealing forms specular and large grain $MAPbI_3$ perovskite. This is suggested to be due to retardation of the crystallisation process favouring greater crystal growth over time. This is evidenced by the control sample which shows a specular film (by eye) with crystal domains visible with a mean average maximum Feret diameter of 346 ± 183 nm under 30 000× magnification. Films cast from candidate solutions give numerous oriented nucleation sites required for the formation of the compact film upon annealing. Due to this action directly impacting the growth phase of the crystallisation, the crystal size visible for candidate solution films appears smaller. Solvent systems A and C produce films with crystal sizes of 267 ± 106 nm and 264 ± 112 nm respectively whereas candidate B shows more comparable average crystal size to the control sample with 304 ± 108 nm.

This suggests that films manufactured using the DMF/DMSO control system consist of larger grained crystals on average (Table S5†). However, the greater standard deviation in the data set, along with size distribution graphs (Fig. S5†), show that there is a skew towards the formation of comparatively small crystals alongside the large grains for this sample. Whilst the average Feret diameter taken for candidate films A–C is lower, the grains tend to a normal distribution and a lower standard deviation from the mean. Analysis of this data, in conjunction with the XRD results suggest that size distri-

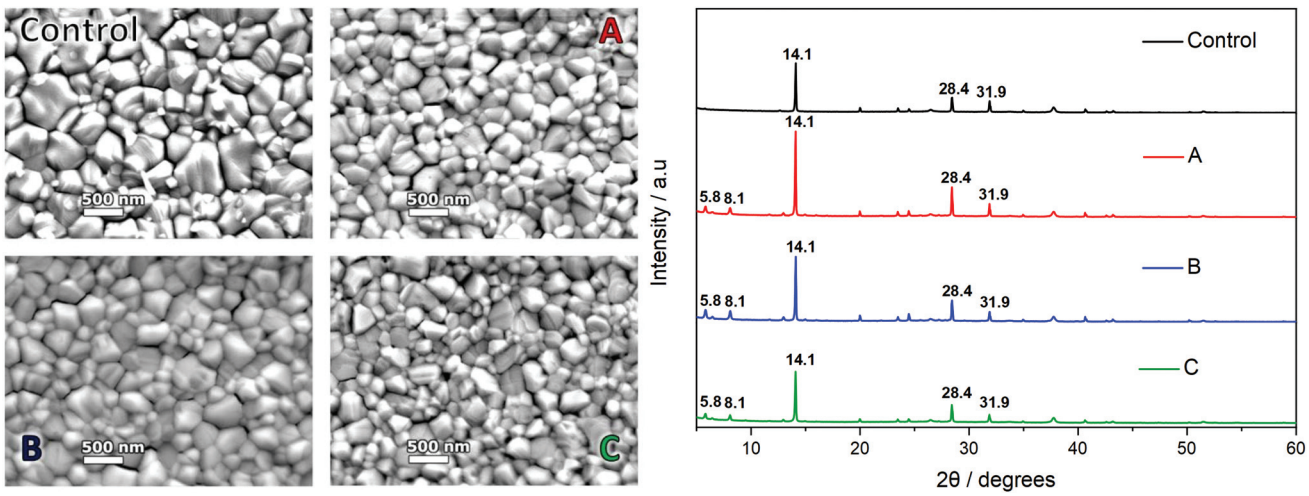


**Fig. 6** Top down 30 000× magnification SEM images for candidate solutions A, B, C, and control (DMF/DMSO 80/20 v/v) (left) and XRD scans for candidate solutions A, B, C, and control (DMF/DMSO 80/20 v/v) (right).

bution, along with film compactness and uniformity, may lead to films with higher crystallinity. This difference is thought to be related to the use of the prenucleation spin coating methodology, where a homogenous spread of nucleation centres initiates the crystal growth in a highly uniform and preferentially regimented manner, tightening the size distribution seen in the final film.

Distinctive tetragonal $MAPbI_3$ peaks can be seen for all samples at 14.1°, 28.4° and 31.9° corresponding to the 110, 220, and 114 crystal planes (Fig. 6, right).[76] For the DMF/DMSO sample a small diffraction peak can be seen at 12.6° attributed to $PbI_2$.[76]

For the candidate solutions a new peak is exhibited at around 13.1° along with other smaller peaks at approximately 15° and 16°, these are likely due to the presence of an intermediate $PbI_2$, similar to those exhibited in the works by Y. Ren *et al.*[77] In this the MAI and solvents are interacting with the layered structure of the $PbI_2$ resulting in a distortion of the $PbI_2$ lattice, most notably in the *c* axis, which presents as a shift in the peak positions.

All candidate solutions also exhibit two prominent peaks and a smaller tertiary peak below 10°. These were identified at 5.8°, 6.5°, and 8.1° respectively. This may be due to the presence of 2D perovskite phases; the use of specific solvents and solvent additives has been reported to produce 2D lattice structures classified by the number of lattice layers *n*.[78] The most likely region for any 2D perovskite growth would be the ETL/PAL interface, due to the spin coating procedure. As the incidence angle is very acute, it remains unlikely that we have identified 2D $MAPbI_3$ perovskite during these XRD scans of 400–500 nm thick samples. Another possible explanation for the observed low angle (<10°) peaks is the presence of solvated phases within the sample. This could be due to an insufficient annealing step, or residual solvent present within the bulk. Although identification of the exact peak position is difficult to match, recent studies – also applying a prenucleation style of drip – identify three low angle peaks as $MA_2Pb_3I_8{\cdot}2DMSO$.[79] The XRD position reported here is shifted to the left by ~1° compared to that presented by Zhang *et al.*, 2020. However, the relative position and intensity of the three peaks show good agreement.[79]

The full width at half maximum (FWHM) of the diffraction peaks were measured (Table S4†) with the DMF/DMSO control providing the baseline for a high quality film. Candidate A, B and the DMF/DMSO sample all show similar FWHM values for the 110 peak (*ca.* 0.09). For both the 220 and 310 peaks the FWHM for candidate A is the lowest of all samples. This, along with the higher PL intensity observed suggests higher crystallinity within the material. This is postulated to be the result of reduced impurities resulting from the use of the prenucleation method with this sample. The intensity of the 110 peak shows a higher intensity in all of the candidate solutions (order of precedence A–B–C–Control) compared to the control, with candidate C showing largest FWHM and consequently the poorest crystallinity, again this agrees with the PL measurements with C producing lower PL intensity compared to A and B. In terms of peak intensity, the 310 peak is noticeably lower relative to the 110 and 220 peaks in the candidate films compared to the DMF/DMSO film. Table S4† shows the 110/310 peak intensity ratio for each solvent system. All candidate solutions show a higher ratio suggesting 110 orientation is dominant. This suggests that the candidate films form crystals with less disorder than the DMF/DMSO derived film and a preferred grain orientation.[80]

### Photovoltaic performance evaluation for candidate solutions

The three candidate precursor solutions produce devices of a similar efficiency to the DMF/DMSO control devices (Table 5) with no discernible performance loss on substituting the harmful DMF-based solvent system with the 'greener' alternatives. Box plots, showing the four photovoltaic parameters PCE, $J_{sc}$, $V_{oc}$, and FF on a pixel by pixel basis can be seen in Fig. S10.† Amongst the candidate solutions (A–C) similar performance may be expected as they do not vary a great deal in composition, however, it does show a degree of flexibility which could be valuable when matching a solvent system to a particular deposition method.

Candidate A in particular matches the performance of the DMF/DMSO system extremely well with the champion devices achieving over 16% PCE matching the champion devices of DMF/DMSO (the *J–V* curves for all champion devices are given in Fig. S8†). For average values Candidates B and C produce overall similar PCE values with slightly lower $J_{SC}$ values which may be due to slightly less uniform films as suggested by the XRD and in the case of Candidate C, lower PL intensity. Candidates B and C also didn't produce as high efficiency

**Table 5** Combined control and candidate system device performance for the four photovoltaic parameters; power conversion efficiency (PCE%), fill factor (FF), open circuit voltage ($V_{oc}$), and short circuit current ($J_{sc}$)

| Solvent system | | PCE/% | $J_{sc}$/mA cm$^{-2}$ | $V_{oc}$/V | FF/% |
|---|---|---|---|---|---|
| DMF/DMSO | Average | 12.4 ± 2.0 | 19.4 ± 1.7 | 0.97 ± 0.04 | 65.6 ± 7.2 |
| | Champion | 16.22 | 22.02 | 0.97 | 75.8 |
| Candidate A | Average | 12.3 ± 1.9 | 19.5 ± 1.7 | 0.97 ± 0.04 | 64.8 ± 7.1 |
| 40% DMSO, 30% DMPU, 20% 2-MeTHF, 10% EtOH | Champion | 16.05 | 21.35 | 0.94 | 79.6 |
| Candidate B | Average | 11.9 ± 1.1 | 17.9 ± 2.1 | 0.97 ± 0.06 | 69.0 ± 3.1 |
| 40% DMSO, 30% DMPU, 15% 2-MeTHF, 15% EtOH | Champion | 13.32 | 20.79 | 0.92 | 69.6 |
| Candidate C | Average | 12.3 ± 1.8 | 18.8 ± 1.0 | 0.99 ± 0.04 | 66.1 ± 7.6 |
| 40% DMSO, 40% DMPU, 10% 2-MeTHF, 10% EtOH | Champion | 13.94 | 18.96 | 1.01 | 67.8 |

champion devices compared to Candidate A and the control DMF/DMSO, although this may just be a case of needing further refinement of the spin coating cycle and anti-solvent drip. Specifically, the addition of increased amounts of EtOH in candidate B and DMPU in candidate C subsequently serves to increase solution supersaturation and reduce film evacuation respectively, both parameters expected to impact deposition.

Based on all the evidence available to us, it seems apparent that Candidate A is the most promising, but B and C could potentially be improved further and the ability to tune the solvent composition without significantly effecting device performance could be extremely valuable to optimising the solvent system to various printing techniques. As an example, candidate solution C could be chosen for experimentation with excess $PbI_2$, a common strategy to increase device PCE, as it has the highest % of DMSO/DMPU (total 80%); by tuning the ratio to include more DMPU and less 2-MeTHF and EtOH blend, the solvating power of the solution is increased potentially allowing increased concentrations of $PbI_2$.

## Conclusions

In this work we have identified a solvent system consisting of DMSO, DMPU, 2-MeTHF and EtOH that is capable of matching the performance of the commonly used DMF/DMSO solvent system for deposition of $MAPbI_3$. We have shown there is a degree of flexibility in the composition of this solvent system by studying three candidate solutions (A–C), with slightly different compositions of the four constituent solvents, that all achieve similar device performance to the control DMF/DMSO. 'Hero' devices produced PCE values of 16.2, 16.1, 13.3, and 13.9% for when DMF/DMSO and A–C are used to deposit $MAPbI_3$ respectively. XRD and SEM confirm that the solvent systems produce dense, crystalline, and uniform films with no observable pin-holes. We have highlighted and demonstrated the methodology for green solvent substitution which we hope will act as a framework to support further development of greener and more sustainable solvent systems for PSC manufacturing and hasten the commercialisation of this technology. We have investigated commercially available solvents and used benchmarks of basicity as represented through the Gutmann donor number, and dielectric constant to identify solvents likely to dissolve $MAPbI_3$ perovskite precursors (MAI and $PbI_2$). Two dipolar aprotic solvents DMSO and DMPU were identified as a cosolvent system capable of forming high (1.25 M) concentration solutions suitable for spin coating. Emphasis was also placed on the increased $Pb^{2+}$ coordinating ability of the DMSO/DMPU system to produce highly crystalline planar perovskite films. An additive cosolvent system comprising the derived 'green' solvent 2-methyltetrahydrofuran and ethanol helped to mitigate over coordination improving film quality and ease of spin coating. A prenucleation style of anti-solvent drip was utilised with a $MAPbI_3$ crystalline film forming during the spin coating process and providing a dense spread of nucleation sites for further temperature induced crystal growth from the solvated phase. Our results suggest that this solvent system results in efficient, compact films with superior fluorescence emission and improved crystallinity compared to the highly optimised DMF/DMSO cosolvent system. Solvent systems A–C produced films with significantly higher fluorescence emission compared to the DMF/DMSO system, with A and B showing the highest fluorescence intensity likely due to the higher volume % of 2-MeTHF (20 and 15% respectively) resulting in slightly thicker films (487 and 492 nm respectively *vs.* 366 nm for DMF/DMSO) while retaining higher crystallinity and uniformity as evidenced by SEM observations. While the 3 candidate solutions presented here have similar compositions, we feel that analysis of these systems highlights the potential for customisable solvent system to alter crystallinity, reduce defects, and tune the properties of the perovskite film and could potentially be optimised for a given manufacturing method. We have used environmental, health and safety considerations (EHS) of the solvents as the first step in screening potentially 'greener' solvents producing a system significantly better than DMF/DMSO in terms of the EHS credentials. Moving forward, thorough techno-economic evaluation and extended lifecycle assessment methodologies should be undertaken to verify that solvent substitution results in reduced environmental impacts throughout the whole lifecycle of PSC devices and no unintended consequences occur from adoption of alternative solvent systems.

## Conflicts of interest

There are no conflicts to declare.

## Acknowledgements

We are grateful for the financial support of the EPSRC (EP/R016666/1 and EP/S001336/1) and both the EPSRC and Innovate UK for the SPECIFIC Innovation and Knowledge Centre and the European Regional Development Fund through the Welsh Government for support to the Sêr Solar program. MLD and TW are grateful for funding through the EPSRC GCRF SUNRISE project (EP/P032591/1). This project has received funding from the European Union Horizon 2020 research and innovation programme under the Marie Sklodowska—Curie grant agreement no 764787. The authors would like to acknowledge the assistance provided by Swansea University College of Engineering AIM Facility, which was funded in part by the EPSRC (EP/M028267/1).

## References

1 A. Kojima, K. Teshima, Y. Shirai and T. Miyasaka, *J. Am. Chem. Soc.*, 2009, **131**, 6050–6051.
2 Best Research-Cell Efficiency Chart | Photovoltaic Research | NREL, https://www.nrel.gov/pv/cell-efficiency.html, (accessed 7 April 2020).

 

3 N. G. Park and K. Zhu, *Nat. Rev. Mater.*, 2020, **5**, 333–350.
4 M. A. Green, E. D. Dunlop, J. Hohl-Ebinger, M. Yoshita, N. Kopidakis and A. W. Y. Ho-Baillie, *Prog. Photovolt. Res. Appl.*, 2020, **28**, 3–15.
5 L. J. Phillips, A. M. Rashed, R. E. Treharne, J. Kay, P. Yates, I. Z. Mitrovic, A. Weerakkody, S. Hall and K. Durose, *Sol. Energy Mater. Sol. Cells*, 2016, **147**, 327–333.
6 M. L. Davies, M. Carnie, P. J. Holliman, A. Connell, P. Douglas, T. Watson, C. Charbonneau, J. Troughton and D. Worsley, *Energy Mater. Mater. Sci. Eng. Energy Syst.*, 2014, **9**, 482–485.
7 Y. Wang, W. Fu, J. Yan, J. Chen, W. Yang and H. Chen, *J. Mater. Chem. A*, 2018, **6**, 13090–13095.
8 S. E. Sofia, H. Wang, A. Bruno, J. L. Cruz-Campa, T. Buonassisi and I. M. Peters, *Sustainable Energy Fuels*, 2020, **4**, 852–862.
9 L. Meng, J. You and Y. Yang, *Nat. Commun.*, 2018, **9**, 1–4.
10 R. G. Charles, M. L. Davies and P. Douglas, *Electronics Goes Green 2016+ (EGG)*, Berlin, Germany, 2016, pp. 1–8.
11 R. G. Charles, M. L. Davies, P. Douglas, I. L. Hallin and I. Mabbett, *Energy*, 2019, **166**, 1207–1215.
12 R. G. Charles, P. Douglas, J. A. Baker, M. J. Carnie, J. O. Douglas, D. J. Penney and T. M. Watson, *J. Cleaner Prod.*, 2018, **202**, 1167–1178.
13 S. Maranghi, M. L. Parisi, R. Basosi and A. Sinicropi, *Energies*, 2019, **12**, 3–7.
14 R. L. Moss, E. Tzimas, H. Kara, P. Willis and J. Kooroshy, *Energy Policy*, 2013, **55**, 556–564.
15 J. Tao and S. Yu, *Sol. Energy Mater. Sol. Cells*, 2015, **141**, 108–124.
16 C. de Castro, M. Mediavilla, L. J. Miguel and F. Frechoso, *Renewable Sustainable Energy Rev.*, 2013, **28**, 824–835.
17 A. Elshkaki and T. E. Graedel, *J. Cleaner Prod.*, 2013, **59**, 260–273.
18 R. G. Charles, P. Douglas, M. Dowling and M. L. Davies, *Resour., Conserv. Recycl.*, 2020, **161**, 104923.
19 M. L. Davies, *Joule*, 2020, **4**, 1626–1627.
20 P. J. Holliman, E. W. Jones, A. Connell, S. Ghosh, L. Furnell and R. J. Hobbs, *Mater. Res. Innovations*, 2015, **19**, 508–511.
21 M. Konstantakou, D. Perganti, P. Falaras and T. Stergiopoulos, *Crystals*, 2017, **7**, 1–21.
22 A. Binek, M. L. Petrus, N. Huber, H. Bristow, Y. Hu, T. Bein and P. Docampo, *ACS Appl. Mater. Interfaces*, 2016, **8**, 12881–12886.
23 J. W. Lee, H. S. Kim and N. G. Park, *Acc. Chem. Res.*, 2016, **49**, 311–319.
24 K. Nishimura, M. A. Kamarudin, D. Hirotani, K. Hamada, Q. Shen, S. Iikubo, T. Minemoto, K. Yoshino and S. Hayase, *Nano Energy*, 2020, **74**, 104858.
25 K. X. Steirer, P. Schulz, G. Teeter, V. Stevanovic, M. Yang, K. Zhu and J. J. Berry, *ACS Energy Lett.*, 2016, **1**, 360–366.
26 L. Serrano-Lujan, N. Espinosa, T. T. Larsen-Olsen, J. Abad, A. Urbina and F. C. Krebs, *Adv. Energy Mater.*, 2015, **5**, 1501119.
27 K. L. Gardner, J. G. Tait, T. Merckx, W. Qiu, U. W. Paetzold, L. Kootstra, M. Jaysankar, R. Gehlhaar, D. Cheyns, P. Heremans and J. Poortmans, *Adv. Energy Mater.*, 2016, **6**, 1–8.
28 J. Wang, F. Di Giacomo, J. Brüls, H. Gorter, I. Katsouras, P. Groen, R. A. J. Janssen, R. Andriessen and Y. Galagan, *Solar RRL*, 2017, **1**, 1700091.
29 W. Y. Tan, P. P. Cheng, Y. W. Zhang, J. M. Liang, X. Chen, Y. Liu and Y. Min, *J. Mater. Chem. C*, 2019, **7**, 6004–6011.
30 M. Lv, X. Dong, X. Fang, B. Lin, S. Zhang, J. Ding and N. Yuan, *RSC Adv.*, 2015, **5**, 20521–20529.
31 Sigma Aldrich, MSDS - 227056, https://www.sigmaaldrich.com/MSDS/MSDS/DisplayMSDSPage.do?country=GB&language=en&productNumber=227056&brand=SIAL&PageToGoToURL=https%3A%2F%2Fwww.sigmaaldrich.com%2Fcatalog%2Fproduct%2Fsial%2F227056%3Flang%3Den, (accessed 7 April 2020).
32 P. J. Holliman, E. W. Jones, A. Connell, S. Ghosh, L. Furnell and R. J. Hobbs, *Mater. Res. Innovations*, 2015, **19**, 508–511.
33 J. Lee and S. Baik, *RSC Adv.*, 2018, **8**, 1005–1013.
34 J. C. Hamill, J. Schwartz and Y. L. Loo, *ACS Energy Lett.*, 2018, **3**, 92–97.
35 Z. Zhou, Z. Wang, Y. Zhou, S. Pang, D. Wang, H. Xu, Z. Liu, N. P. Padture and G. Cui, *Angew. Chem., Int. Ed.*, 2015, **54**, 9705–9709.
36 J. Zhang, G. B. White, M. D. Ryan, A. J. Hunt and M. J. Katz, *ACS Sustainable Chem. Eng.*, 2016, **4**, 7186–7192.
37 C. Capello, U. Fischer and K. Hungerbühler, *Green Chem.*, 2007, **9**, 927–934.
38 U. Tilstam, *Org. Process Res. Dev.*, 2012, 1273–1278.
39 B. J. Kim, D. H. Kim, S. L. Kwon, S. Y. Park, Z. Li, K. Zhu and H. S. Jung, *Nat. Commun.*, 2016, **7**, 1–9.
40 C. M. Alder, J. D. Hayler, R. K. Henderson, A. M. Redman, L. Shukla, L. E. Shuster and H. F. Sneddon, *Green Chem.*, 2016, **18**, 3879–3890.
41 P. G. Jessop, *Green Chem.*, 2011, **13**, 1391–1398.
42 F. P. Byrne, S. Jin, G. Paggiola, T. H. M. Petchey, J. H. Clark, T. J. Farmer, A. J. Hunt, C. Robert McElroy and J. Sherwood, *Sustainable Chem. Processes*, 2016, **4**, 7.
43 D. Prat, O. Pardigon, H. W. Flemming, S. Letestu, V. Ducandas, P. Isnard, E. Guntrum, T. Senac, S. Ruisseau, P. Cruciani and P. Hosek, *Org. Process Res. Dev.*, 2013, **17**, 1517–1525.
44 N. G. Anderson, *Pract. Process Res. Dev.*, 2010, 81–111.
45 L. J. Diorazio, D. R. J. Hose and N. K. Adlington, *Org. Process Res. Dev.*, 2016, **20**, 760–773.
46 K. Alfonsi, J. Colberg, P. J. Dunn, T. Fevig, S. Jennings, T. A. Johnson, H. P. Kleine, C. Knight, M. A. Nagy, D. A. Perry and M. Stefaniak, *Green Chem.*, 2008, **10**, 31–36.
47 D. Prat, J. Hayler and A. Wells, *Green Chem.*, 2014, **16**, 4546–4551.
48 C. J. Clarke, W. C. Tu, O. Levers, A. Bröhl and J. P. Hallett, *Chem. Rev.*, 2018, **118**, 747–800.
49 J. L. Scott and H. F. Sneddon, *Green Techniques for Organic Synthesis and Medicinal Chemistry*, ed. W. Zhang and B. Cue, John Wiley & Sons, 2nd edn, 2018, ch. 2, vol. 1, pp. 21–42.

50 D. Prat, A. Wells, J. Hayler, H. Sneddon, C. R. McElroy, S. Abou-Shehada and P. J. Dunn, *Green Chem.*, 2015, **18**, 288–296.
51 S. Abbott, C. M. Hansen, H. Yamamoto and R. S. Valpey, *Hansen Solubility Parameters in Practice Complete with eBook, software and data 5th Edition The HSPiP team*, 2015.
52 N. K. Noel, S. N. Habisreutinger, B. Wenger, M. T. Klug, M. T. Hörantner, M. B. Johnston, R. J. Nicholas, D. T. Moore and H. J. Snaith, *Energy Environ. Sci.*, 2017, **10**, 145–152.
53 N. J. Jeon, J. H. Noh, Y. C. Kim, W. S. Yang, S. Ryu and S. Il Seok, *Nat. Mater.*, 2014, **13**, 897–903.
54 Q. Liu, Y. Zhao, Y. Ma, X. Sun, W. Ge, Z. Fang, H. Bai, Q. Tian, B. Fan and T. Zhang, *J. Mater. Chem. A*, 2019, **7**, 18275–18284.
55 K. H. Hendriks, J. J. Van Franeker, B. J. Bruijnaers, J. A. Anta, M. M. Wienk and R. A. J. Janssen, *J. Mater. Chem. A*, 2017, **5**, 2346–2354.
56 X. Fang, Y. Wu, Y. Lu, Y. Sun, S. Zhang, J. Zhang, W. Zhang, N. Yuan and J. Ding, *J. Mater. Chem. C*, 2017, **5**, 842–847.
57 D. Burkitt, P. Greenwood, K. Hooper, D. Richards, V. Stoichkov, D. Beynon, E. Jewell and T. Watson, *MRS Adv.*, 2019, **4**, 1399–1407.
58 D. Burkitt, R. Patidar, P. Greenwood, K. Hooper, J. McGettrick, S. Dimitrov, M. Colombo, V. Stoichkov, D. Richards, D. Beynon, M. Davies and T. Watson, *Sustainable Energy Fuels*, 2020, **4**, 3340–3351.
59 Y. Deng, C. H. van Brackle, X. Dai, J. Zhao, B. Chen and J. Huang, *Sci. Adv.*, 2019, **5**, 1–9.
60 A. Babaei, L. Albero-Blanquer, A. M. Igual-Muñoz, D. Pérez-Del-Rey, M. Sessolo, H. J. Bolink and R. Tadmouri, *Polyhedron*, 2018, **147**, 9–14.
61 H. Team, H. Yamamoto, S. Abbott and C. M. Hansen, Hansen Solubility Parameters 50th anniversary conference, preprint PP, 2017.
62 P. Loubet, M. Tsang, E. Gemechu, A. Foulet and G. Sonnemann, in *Bio-based solvents*, ed. F. Jérôme and R. Luque, John Wiley & Sons, Ltd, Chichester, UK, 2017, pp. 131–148.
63 W. Ke, G. Fang, Q. Liu, L. Xiong, P. Qin, H. Tao, J. Wang, H. Lei, B. Li, J. Wan, G. Yang and Y. Yan, *J. Am. Chem. Soc.*, 2015, **137**, 6730–6733.
64 Z. Wei, B. Smith, F. De Rossi, J. R. Searle, D. A. Worsley and T. M. Watson, *J. Mater. Chem. C*, 2019, **7**, 10981–10987.
65 P. F. Méndez, S. K. M. Muhammed, E. M. Barea, S. Masi and I. Mora-Seró, *Solar RRL*, 2019, **3**, 1900191.
66 M. Saliba, J.-P. Correa-Baena, C. M. Wolff, M. Stolterfoht, N. Phung, S. Albrecht, D. Neher and A. Abate, *Chem. Mater.*, 2018, **30**, 4193–4201.
67 A. Way, J. Luke, A. D. Evans, Z. Li, J. S. Kim, J. R. Durrant, H. K. Hin Lee and W. C. Tsoi, *AIP Adv.*, 2019, **9**, 085220.
68 E. V. Péan, C. S. De Castro and M. L. Davies, *Mater. Lett.*, 2019, **243**, 191–194.
69 R. Vidal, J.-A. Alberola-Borràs, G.-M. Joaquín-Luis, S. N. Habisreutinger, D. T. Moore, T. H. Schloemer, I. Mora-Seró, J. J. Berry and J. M. Luther, *Nat. Sustain.*, 2021, **4**, 227–285.
70 B. S. Flowers, M. S. Mittenthal, A. H. Jenkins, D. A. Wallace, J. W. Whitley, G. P. Dennis, M. Wang, C. H. Turner, V. N. Emel'Yanenko, S. P. Verevkin and J. E. Bara, *ACS Sustainable Chem. Eng.*, 2017, **5**, 911–921.
71 D. Lundberg, *The Coordination Chemistry of Solvated Metal Ions in DMPU A Study of a Space-Demanding Solvent*, 2006.
72 S. Rahimnejad, A. Kovalenko, S. M. Forés, C. Aranda and A. Guerrero, *ChemPhysChem*, 2016, 2795–2798.
73 I. Persson, K. Lyczko, D. Lundberg, L. Eriksson and A. Pjaczek, *Inorg. Chem.*, 2011, **50**, 1058–1072.
74 F. Cataldo, *Eur. Chem. Bull.*, 2015, **4**, 92–97.
75 H. H. Khoo, L. L. Wong, J. Tan, V. Isoni and P. Sharratt, *Resour., Conserv. Recycl.*, 2015, **95**, 174–182.
76 P. Chhillar, B. P. Dhamaniya, V. Dutta and S. K. Pathak, *ACS Omega*, 2019, **4**, 11880–11887.
77 Y. Ren, B. Duan, Y. Xu, Y. Huang, Z. Li, L. Hu, T. Hayat, H. Wang, J. Zhu and S. Dai, *Sci. China Mater.*, 2017, **60**, 392–398.
78 Y. Hu, L. M. Spies, D. Alonso-Álvarez, P. Mocherla, H. Jones, J. Hanisch, T. Bein, P. R. F. Barnes and P. Docampo, *J. Mater. Chem. A*, 2018, **6**, 22215–22225.
79 K. Zhang, Z. Wang, G. Wang, J. Wang, Y. Li, W. Qian, S. Zheng, S. Xiao and S. Yang, *Nat. Commun.*, 2020, **11**, 1–11.
80 C. Jiang, Y. Xie, R. R. Lunt, T. W. Hamann and P. Zhang, *ACS Omega*, 2018, **3**, 3522–3529.